**Title**
DNA Segregation on Bacteria: Partitioning of the R1 Plasmid



**Author**
Campbell, Christopher

**Publication Date**
2008-03-04

Peer reviewed|Thesis/dissertation

# Bacterial DNA Segregation: Partitioning of the R1 Plasmid

by

Christopher S Campbell

DISSERTATION

Submitted in partial satisfaction of the requirements for the degree of

DOCTOR OF PHILOSOPHY

in

Biochemistry

in the

GRADUATE DIVISION

of the

# Dedication

This is for Lucy

## Acknowledgements

Chapters 2 and 4 of this thesis is a reprint of the material as it appears in Science and the Journal of Cell Biology respectively. The co-author listed in this publication directed and supervised the research that forms the basis for the thesis.

# Abstract

Although the mechanism of DNA segregation in Eukaryotes has been known for many decades, Prokaryotic DNA segregation has remained a mystery. I have studied a form of plasmid segregation in bacteria in order to get a better understanding of this process. The R1 Par operon is a self-contained plasmid partitioning system composed of three parts: *parC*, ParR and ParM. *parC* is a stretch of DNA consisting of 10 sequential repeats, each of which binds ParR. The ParR/*parC* complex in turn binds the actin homolog ParM. Previous studies have shown that ParM forms filaments nearly identical to those of eukaryotic actin filaments and that ParM filament bundles appear to position plasmids at each end of a rod-shaped cell. We demonstrate that ParM filaments are dynamically unstable and can elongate bidirectionally *in vitro*. ParM filaments also nucleate at a speed much faster than that of eukaryotic actins. Addition of ParR and *parC* coated beads induced long bundles of filaments with a bead at each end, indicating that the ParR/*parC* complex can suppress ParM dynamic instability. ParM filaments are also dynamically unstable *in vivo* and that the majority of filaments undergo assembly and rapid disassembly in less than a minute. These observations led to a model in which ParM filaments continually search the cytoplasm and eventually capture a ParR bound *parC* region on a plasmid. Insertional polymerization at the ParM/ParR interface will then push the plasmids to opposite ends of the cell and hold them in place until cell division, ensuring that each daughter cell receives a copy.

# Table of Contents

# Chapter 1

DNA segregation is one of the most vital tasks of all life on earth. Oddly enough, for the vast majority of organisms, we have no idea whatsoever how it is accomplished. For over a century now, the basic mechanism of chromosome segregation in Eukaryotes has been well understood. Spindle fibers attach to the kintetochore of a chromosome and pull them to each end of the cell before division. In bacteria, the process was a complete mystery when I started working on this project. There were theories about chromosomes being pushed apart by the cell wall or DNA replication. These theories were based on nothing but speculation, but they were grasped onto simply because there's been nothing else to replace them with.

Things only started to change in the late nineteen nineties when it was revealed that bacteria contain polymers similar to those of Eukaryotes. Over the past decade, new bacterial polymers have been discovered at an extreme pace. Consider: the first, FtsZ, was first shown to polymerize in 1996 (Erickson 1996). We now know of over a dozen distinct polymer-forming proteins in as many bacterial species, the majority of which are distant relatives of tubulin and actin. It did not take long for scientists to speculate that these proteins would play similar roles to their Eukaryotic counterparts, namely spatial regulation. Chief among these functions is DNA segregation, as is accomplished by microtubules.

As I mentioned before, FtsZ was the first protein polymer to be characterized in bacteria. It is a tubulin homolog that forms short filaments around the center of the cell prior to septation (Ma 1996). Its primary function is thought to be that of a scaffold,

providing a docking site for a variety of proteins that are involved in cell division. Without FtsZ, cells become filamentous as they continue to grow without being able to divide.

Another major bacterial protein polymer that is found in a large variety of bacteria is MinD. MinD is responsible for ensuring the proper localization of FtsZ at the midcell. It oscillates back and forth between the poles of the cell, where its binding partner, MinC, depolymerizes FtsZ. MinD forms some sort of polymer that is negatively regulated by MinE (Johnson 2002). Cells that are mutant for any of the Min proteins sometimes divide at the ends, making small, "mini" cells, which is how they were first identified.

The next protein to enter the bacterial cytoskeleton field was the actin homolog MreB. MreB was first shown to form filaments in cells by Jeff Errington's Lab. They observed helices in Bacillus subtlis that wound around the inside of the membrane (Jones 2001). Shortly thereafter, Fucinita van den Ent observed filaments by EM with purified MreB from T. maritima. The structure of the filaments was dissimilar to actin, in that the protofilaments were straight instead of wrapped around each other in a helix. However, in the same paper, they revealed the crystal structure of MreB, which had many unmistakable similarities to the structure of actin (van den Ent 2001). MreB seems to serve a variety of functions, most notably in cell wall synthesis. Depletion of MreB causes rod-shaped cells to become round, as they are no longer able to retain their shape without the rigidity the cell wall provides. MreB has also been strongly implicated in chromosome segregation, though its specific role in the process is still unclear (Gitai 2005).

The fourth bacterial polymer that is common to many types of bacteria is ParA. ParA is a Walker box-type ATPase found on some chromosomes and plasmids. It is involved in DNA segregation along with ParB, a DNA binding protein, which binds to parC sites near the parAB operon. ParAs form bundles of filaments in vitro, and whose polymerization kinetics are affected by ParB (Barilla 2007). The mechanism by which the ParA/B system increases the transmission frequency of the DNA on which it is encoded is undnkown. Recent evidence has suggested that depolymerizing ParA polymer pulls one chromosome or plasmid away from the other (Yamaichi 2007).

Those four proteins (FtsZ, MreB, MinD, and ParA) are thus far the only bacterial cytoskeletal proteins found in a large variety of bacteria. There are many other bacterial polymers that are found only in specific species and plasmids. I will briefly discuss six of them: ParM, AlfA, MamK, BtubA and B, TubZ, and CreS.

ParM is an actin homolog that has been extensively studied by the Gerdes group in Denmark. ParM forms filaments in bacteria that are responsible for the segregation of low-copy plasmids. This protein is the focus of this thesis and will be discussed more thoroughly below.

AlfA is another bacterial plasmid segregating actin. Found in Bacillus, AlfA forms filaments in cells (Becker 2006). Not much else is known, as only one paper has been published on the protein. The last actin homolog is MamK. MamK is found in magnetotactic bacteria and is involved in coordinating magnetosomes in a straight line along the length of the bacterium. This proper alignment of the megnetosomes is necessary for the bacteria's magnetotctic capabilities (Komeili 2006). No biochemical work on MamK has been published.

There are two other bacterial tubulins that have been identified (aside from FtsZ). TubA and TubB are much more closely related to eukaryotic tubulin than any of the other bacterial homologs (close to 40% sequence identity). They also have two subunits, like their Eukaryotic counterpart. Nothing is known about them functionally, but they have been crystallized and shown to have a remarkably similar fold to alpha and beta tubulin (Schlieper 2005). The third tubulin homolog is TubZ. Like many of the other bacterial polymers, TubZ is involved in plasmid segregation. It has been seen to treadmill around the inside of the cell membrane (Larsen 2007). How this leads to plasmid segregation is anyone's guess.

Last but not least is the Caulobacter crescentus protein CreS. CreS is necessary to give C. crescentus its crescent shape. It forms intermediate filaments that localizes to the inside of the curved part of the cell. It is interesting to note that with the discovery of CreS, all three of the Eukaryotic cytoskeleton families (tubulin, actin, and intermediate filaments) are represented in bacteria.

That's all the prokaryotic cytoskeletal filaments that have been published to date. Let's focus more on ParM. ParM is one of two proteins present in an operon in a variety of low-copy plasmids found in enteric bacteria. The other is ParR. ParR is a DNA binding protein that binds specifically to a sequence surrounding the operon's promoter, called parC. All of the early work on the system was pure genetics. They discovered things like that ParM and ParR can act in trans whereas parC must be in cis with the plasmid that's being stabilized. Also, parC is incompatible with other plasmids that also contain parC. All these things would have been easily predicted based on what we know now, so I won't go into great detail about them.

Back in the early 1970s, when plasmid research was still popular, Kurt Nordstrom was studying a plasmid called R1 and determining its copy number and stability of inheritance. At that point, it was clear that there were mechanisms inherent to the plasmid that prevented its loss. It wasn't until the mid 1980s when Kenn Gerdes began to study the plasmid in Soren Molin's lab that the regions responsible were identified. In 1985, Kenn isolated an area of the plasmid that was sufficient to stabilize other low copy plasmids around a thousand fold. Then, in 1986, he further divided the region into two sub-regions that could each stabilize the plasmid a hundred fold. He named the regions parA and parB (par for partition). parB turned out to be a system called either host killing or plasmid addiction. It does not involve a cytoskeletal filament, so I will ignore it. ParA is now named the R1 par operon, which contains parC, parR and parM. More specifics on the backround of the R1 par operon will be presented in the introductions to Chapters 2 and 4.

Barilla, D., E. Carmelo, and F. Hayes. 2007. The tail of the ParG DNA segregation protein remodels ParF polymers and enhances ATP hydrolysis via an arginine finger-like motif. *Proc Natl Acad Sci U S A*. 104:1811-6.

Becker, E., N.C. Herrera, F.Q. Gunderson, A.I. Derman, A.L. Dance, J. Sims, R.A. Larsen, and J. Pogliano. 2006. DNA segregation by the bacterial actin AlfA during Bacillus subtilis growth and development. *Embo J*. 25:5919-31.

Erickson, H.P., and D. Stoffler. 1996. Protofilaments and rings, two conformations of the

tubulin family conserved from bacterial FtsZ to alpha/beta and gamma tubulin. *J Cell Biol*. 135:5-8.

Gitai, Z., N.A. Dye, A. Reisenauer, M. Wachi, and L. Shapiro. 2005. MreB actin-mediated segregation of a specific region of a bacterial chromosome. *Cell*. 120:329-41.

Johnson, J.E., L.L. Lackner, and P.A. de Boer. 2002. Targeting of (D)MinC/MinD and (D)MinC/DicB complexes to septal rings in Escherichia coli suggests a multistep mechanism for MinC-mediated destruction of nascent FtsZ rings. *J Bacteriol*. 184:2951-62.

Jones, L.J., R. Carballido-Lopez, and J. Errington. 2001. Control of cell shape in bacteria: helical, actin-like filaments in Bacillus subtilis. *Cell*. 104:913-22.

Komeili, A., Z. Li, D.K. Newman, and G.J. Jensen. 2006. Magnetosomes are cell membrane invaginations organized by the actin-like protein MamK. *Science*. 311:242-5.

Larsen, R.A., C. Cusumano, A. Fujioka, G. Lim-Fong, P. Patterson, and J. Pogliano. 2007. Treadmilling of a prokaryotic tubulin-like protein, TubZ, required for plasmid stability in Bacillus thuringiensis. *Genes Dev*. 21:1340-52.

Schlieper, D., M.A. Oliva, J.M. Andreu, and J. Lowe. 2005. Structure of bacterial tubulin BtubA/B: evidence for horizontal gene transfer. *Proc Natl Acad Sci U S A*. 102:9170-5.

van den Ent, F., L.A. Amos, and J. Lowe. 2001. Prokaryotic origin of the actin cytoskeleton. *Nature*. 413:39-44.

Yamaichi, Y., M.A. Fogel, S.M. McLeod, M.P. Hui, and M.K. Waldor. 2007. Distinct centromere-like parS sites on the two chromosomes of Vibrio spp. *J Bacteriol*. 189:5314-24.

# Chapter 2

Recent work suggests that proteins related to eukaryotic actins (1–3) may be involved in prokaryotic chromosome segregation. Another example of prokaryotic DNA segregation, one that has been characterized in molecular detail, is the partitioning of R1 and R100 drug-resistance plasmids. These 100-kb plasmids are found in many enteric pathogens and encode genes that confer antibiotic and heavy-metal resistance as well as genes required for plasmid retention and conjugative transfer. They are stably maintained at two to four copies per cell (4) and have evolved an efficient mechanism to ensure inheritance by both daughters during cell division. The R1 par operon appears to construct a minimalist mitotic spindle from three components—parC, ParR, and ParM (5–7)—that positions pairs of plasmids at opposite ends of a rod-shaped bacterium (8). parC is a stretch of centromeric DNA that includes the R1 par promoter sequence (9); ParR is a repressor protein that binds to the parC locus (9); and ParM is an actin homolog. Purified ParM polymerizes in an ATP-dependent manner (7) into two-stranded helical filaments similar to conventional actin filaments (10) and binds specifically to the ParR-parC complex (8). In vivo, ParM filaments form a bundle that extends the length of the bacterium with plasmid DNA localized at each end, and polymerization of ParM has been postulated to provide force to push plasmids to opposite poles of the cell (7, 8). Because the system contains only three components, we hypothesized that the intrinsic assembly dynamics of ParM are critical to its role in segregating DNA.

We first investigated the kinetic polarity of ParM filament assembly by performing dual-color fluorescence microscopy on ParM filaments assembled in vitro. Both actin filaments and microtubules are structurally and kinetically polarized so that one end of the polymer elongates faster than the other, and ultrastructural studies indicate that ParM filaments have a structural polarity similar to that of actin filaments (10). We polymerized filaments labeled with Alexa 488 (green) by adding the nonhydrolyzable ATP analog adenylylimidodiphosphate (AMP-PNP), and then added Cy3-labeled (red) ParM. Most filaments observed (91%) had green centers with equal amounts of red fluorescence on each end (Fig. 1A); this result suggested that, unlike previously characterized nucleotide-dependent polymers, ParM filament polymerization is kinetically symmetrical.

We next examined the polymerization dynamics of individual ParM filaments by total internal reflection fluorescence (TIRF) microscopy of Alexa 488–labeled ParM. In the presence of AMP-PNP, ParM filaments were very long (Fig. 1B, left) and grew symmetrically with equal rates of assembly at each end (Fig. 1C) (movies S1 and S2). Electron microscopy of polymeric ParM revealed well-separated, individual filaments with no obvious bundles (7, 10). This observation, together with the approximately uniform fluorescence along the length of labeled ParM filaments, implies that we are observing individual filaments and not antiparallel bundles of asymmetrically elongating filaments. In the presence of hydrolyzable ATP, ParM filaments also elongated symmetrically but were much shorter (Fig. 1B, right) and more dynamic (movies S3 to S5). After growing for a variable length of time, ATP-ParM filaments abruptly switched

from bidirectional elongation to rapid, endwise disassembly (Fig. 1D). In most cases disassembly was unidirectional, and in all cases observed (n > 530), the switch from elongation to shortening resulted in complete disassembly of the filament. Shortening did not reflect detachment of the filament from the coverslip, as detachment resulted in disappearance of the filament in a single step (11). At all ParM concentrations above 2 $\mu$M the average filament length was 1.5 $\mu$m, which suggests that length is determined primarily by an intrinsic property of the filaments (Fig. 1F). ATP-ParM filaments elongated with a rate constant of 5.3 ± 1.3 $\mu$M–1 s–1 (n = 50) at each end, similar to that of the fast-growing barbed end of actin filaments. After switching from growth to shortening, filaments disassembled at a rate of 64 ± 20 s–1 (n = 16) (Fig. 1E). The time spent growing and the maximum length achieved before catastrophic disassembly were variable, which suggests that the switch from elongation to shortening is stochastic. This property of switching between phases of elongation and rapid shortening, known as dynamic instability (12), has until now been observed only in eukaryotic microtubules.

ParM filaments, like microtubules and conventional actin filaments, assemble via a nucleation-condensation mechanism characterized by (i) the existence of a critical concentration, above which polymer forms and below which it does not, and (ii) a concentration-dependent time lag in spontaneous polymerization, during which stable nuclei assemble. We used fluorescence resonance energy transfer (FRET) to monitor ParM polymerization kinetics at varying concentrations of protein and ATP [see (11) for assay conditions and control experiments]. Using both FRET and high-speed pelleting assays, we determined an apparent steady-state critical concentration of 2.3 $\mu$M for

Mg2+-ATP ParM (see below) (fig. S3A). This value is consistent with estimates based on fluorescence microscopy (Fig. 1F). In addition, ATP-induced polymerization of ParM filaments proceeded after a time lag that decreased with increasing protein concentration (Fig. 2A, inset) (fig. S3B).

We define the filament nucleus as the smallest oligomer more likely to elongate than to fall apart. By this definition, the maximum rate of polymer assembly is approximately ke+kn+ [m*]n, where [m*] is the initial monomer concentration minus the critical concentration, ke+ is the rate constant for polymer elongation, kn+ is the rate constant for the nucleation reaction, and n is the number of monomers required to form a nucleus (13). By plotting the logarithm of the maximum rate of polymerization versus the logarithm of the protein concentration (13, 14), we determined that conventional actin and ParM both elongate from a nucleus composed of three monomers (Fig. 2A), as expected for a two-stranded, helical polymer (15). Although the slopes are identical, the ParM polymerization data are shifted upward by about 2.5 log units relative to the data for conventional actin. This indicates that the product of the nucleation and elongation rates is higher for ParM than for actin by a factor of 300. Because the elongation rates are approximately equal, the shift in the ParM data must reflect a spontaneous nucleation rate 300 times the rate for conventional actin.

Consistent with previous studies (7), we found that the half-life of ParM filaments in solution increased linearly with increasing concentration of ATP, which suggests that polymer stability is regulated by ATP hydrolysis (Fig. 2B). The bulk assembly kinetics of

ParM were triphasic, with an initial peak in polymer concentration followed by a dip and then a slow approach to equilibrium [see (11) for further discussion of polymerization kinetics]. The initial rise and fall in ParM polymer appears to represent a population of rapidly nucleated filaments that elongate in synchrony and undergo somewhat synchronous catastrophe. Microtubules exhibit similar synchronous behavior under conditions where nucleation is fast and/or nucleotide dissociation is slow (16, 17).

Consistent with the notion that ATP hydrolysis regulates ParM filament stability, we found that ADP-ParM filaments are extremely unstable, with a critical concentration of ~100 $\mu$M (18). To determine whether hydrolysis of ATP itself or dissociation of cleaved phosphate destabilizes the filament, we tested the effect of beryllium fluoride (BeF3), a phosphate analog, on ParM filament stability. BeF3 hasbeenusedtostabilize ADP actin filaments (19), and it appears to induce a conformation similar to that of filaments after cleavage of the {gamma}-phosphate of the bound ATP but before phosphate dissociation (ADP-Pi). Addition of BeF3 and ADP did not induce assembly of ParM filaments, but BeF3 did stabilize filaments formed in low concentrations of ATP (Fig. 2C). TIRF microscopy revealed that the length distribution of BeF3-ParM filaments was identical to that of ATP-ParM filaments (fig. S1A), but BeF3-ParM filaments did not exhibit dynamic instability (movie S6). By FRET assays, the critical concentration of BeF3-ParM is 0.6 $\mu$M (Fig. 3B). It appears that the steady-state monomer concentration that we measure for ATP ParM (2.3 $\mu$M) is the sum of the critical concentrations of the ATP- and ADP-filament ends weighted by their relative abundance.

Polymerization of ParM stimulates hydrolysis of bound ATP (7), so we directly compared the kinetics of ParM polymerization and ATP hydrolysis in side-by-side assays. To measure polymerization, we mixed labeled ParM (15 $\mu$M) with 200 $\mu$M ATP in a rapid mixer and recorded the FRET signal (Fig. 2D). To measure hydrolysis, we mixed material from the same sample with 200 $\mu$M ATP doped with {gamma}-[32P]ATP in a quenched-flow rapid mixing device. Hydrolysis followed filament assembly, and the instantaneous rate of hydrolysis was proportional to the measured polymer concentration (Fig. 2D, inset). The hydrolysis stimulated by polymerization was rapid, with a rate constant of 0.2 s–1. This is similar to the rates of hydrolysis in actin filaments (0.3 s–1) (20) and in polymers of the bacterial tubulin homolog ftsZ (0.13 s–1) (21) and is fast enough to account for the observed rapid dynamics of ParM filaments. Complete loss of ParM polymer did not correlate with complete exhaustion of ATP in the reaction, which suggests that low concentrations of ADP generated in the reaction inhibit polymerization of ParM. Further work revealed that free ADP affects ParM filament stability (11). All of our observations of intrinsic dynamic instability were made under conditions where this additional ADP-dependent destabilizing effect was not observed.

To determine conclusively whether nucleotide hydrolysis drives dynamic instability of ParM filaments, we mutated residues required for ATP hydrolysis by ParM and tested the effect on filament stability. On the basis of the model of Vorobiev et al. for ATP hydrolysis by actin (22), we mutated Glu148 of ParM to Ala (fig. S4A) and tested the effect on polymerization and ATP hydrolysis (11). This mutation (E148A) abolished all detectable ATPase activity, even at high protein concentrations (Fig. 3A, inset). Like

wild-type ParM, the E148A mutant assembled into filaments in a symmetrical bidirectional manner (movie S7); however, unlike wild-type ParM, E148A filaments were stable in low ATP concentrations (Fig. 3A). TIRF microscopy revealed that E148A-ParM filaments are long and stable in the presence of ATP, similar to wild-type ParM filaments formed in the presence of AMP-PNP (fig. S4B). Nucleation of E148A-ParM filaments was slower than that of wild-type filaments, but once formed, mutant filaments elongated at the same rate as wild-type filaments (fig. S4D). Finally, the critical concentration of the E148A mutant (0.68 $\mu$M) was close to that of BeF3-bound wild-type ParM (0.6 $\mu$M) (Fig. 3B).

A basic assumption of nucleotide-dependent dynamic instability is that the polymer is stable as long as the ends retain a cap of nucleotide triphosphate–bound monomers (23, 24). Once this cap is lost, the polymer rapidly depolymerizes. To determine whether ParM filaments are stabilized by an ATP cap, we mixed wild-type and E148A ParM in different ratios to determine whether substoichiometric amounts of E148A can stabilize wild-type ParM filaments. In pelleting experiments, small amounts of E148A decreased the critical concentration of wild-type ParM (Fig. 3C). Above 20% E148A, the total amount of ParM in the supernatant fraction remained constant and was close to the measured critical concentration of the E148A mutant. This result suggests that subsaturating amounts of ATP-bound ParM can stabilize wild-type polymer, consistent with the ability of an ATP cap to stabilize ADP-bound filaments.

TIRF microscopy assays also revealed that small amounts of E148A ParM affects filament stability. Filaments doped with 20% E148A were very stable (fig. S4C) and elongated in a bipolar fashion, similar to filaments composed entirely of E148A (movie S8). Samples with 10% E148A contained a subset of filaments that remained stable for long periods of time. At 3% and 5% E148A, fewer filaments were stable, and samples doped with 1% E148A were identical to wild-type ParM. At dopings of 3% and 5%, we observed filaments that experienced periods of elongation and rapid shortening but did not undergo complete disassembly (Fig. 3D). This behavior is similar to the phenomenon of "rescue" observed in dynamic instability of microtubules.

We note three important differences between the kinetics of ParM filament assembly and those of conventional actin. First, the rate of dissociation of ADP-ParM monomers from filament ends is about 100 times the rate for ADP-actin monomers from the pointed end (Table 1). ADP-actin filaments require severing factors such as cofilin to promote complete disassembly (25), whereas the fast off-rate of ADP-ParM monomers from the end of the filament produced a microtubule-like dynamic instability (Fig. 4A). Second, the nucleation rate of ParM filaments is 300 times the rate for actin filaments. Evolution has erected a large kinetic barrier to spontaneous nucleation of eukaryotic actins, so that actin requires nucleation factors such as the Arp2/3 complex (26) and formins (27) to form filaments in vivo. The rate of the spontaneous ParM filament formation is similar to that of conventional actin in the presence of formins (28). Third, the rate of ADP dissociation from ParM monomers is 100 times as fast as from actin, which requires profilin to achieve the same rate of nucleotide dissociation and exchange

(25). Thus, ParM appears to be kinetically tuned to operate independently of exogenous nucleation, depolymerization, and nucleotide exchange factors.

Both ParM filaments and microtubules segregate DNA, and both exhibit dynamic instability. Dynamic instability of tubulin is driven by guanosine triphosphate hydrolysis; during mitosis, dynamic instability enables the ends of microtubules to search intracellular space efficiently and to locate kinetochores of unattached chromosomes [for a review, see (29)]. Dynamic instability of ParM filaments is driven by ATP hydrolysis, and mutations in ParM that perturb nucleotide hydrolysis abolish plasmid partitioning (30, 31), which suggests that ParM dynamic instability is required for plasmid segregation. We hypothesize that ParM dynamic instability enables filament ends to efficiently locate and capture plasmid DNA targets. The average length of ATP-ParM filaments (1.5 $\mu$m) is comparable to the length of many rod-shaped bacteria, so ParM filaments may be kinetically tuned to search the volume of a bacterial cell and capture ParR-parC complexes. In addition, bidirectional assembly would promote segregation without requiring antiparallel filaments to slide past each other.

Møller-Jensen et al. (7) reported that the ParR-parC complex nucleates ParM polymerization. Their data, however, show only that ParR-parC can stabilize ParM filaments below the steady-state ATP critical concentration. Given the low nucleation barrier and high cellular concentrations of ParM (12 to 14 $\mu$M) (7), nucleation is unlikely to be the point at which ParM assembly is regulated. It appears that the property of ParM kinetics most amenable to regulation is filament stability. We propose that, at cellular

concentrations of ParM, spontaneous nucleation and filament elongation occur throughout the cell, and that these filaments will spontaneously disassemble unless they are stabilized by interaction with ParR-parC (8). In this model, only filaments with plasmid bound to both ends are stabilized against catastrophic disassembly (7, 8), and bidirectional elongation of ParM filaments at the interface with the ParR-parC complex drives plasmid segregation (Fig. 4B). Such insertional polymerization mechanisms have been proposed for elongating microtubule ends attached to kinetochores and actin filaments bound to formin-family proteins.

References

1. T. Kruse, J. Møller-Jensen, A. Løbner-Olesen, K. Gerdes, EMBO J. 22, 5283 (2003).

2. H. J. Soufo, P. L. Graumann, Curr. Biol. 13, 1916 (2003).

3. Z. Gitai, N. Dye, L. Shapiro, Proc. Natl. Acad. Sci. U.S.A. 101, 8643 (2004).

4. K. Nordstro¨ m, L. C. Ingram, A. Lundba¨ ck, J. Bacteriol. 110, 562 (1972).

5. K. Gerdes, S. Molin, J. Mol. Biol. 190, 269 (1986).

6. K. Gerdes, J. E. Larsen, S. Molin, J. Bacteriol. 161, 292 (1985).

7. J. Møller-Jensen, R. B. Jensen, J. Lowe¨ , K. Gerdes, EMBO J. 21, 3119 (2002).

8. J. Møller-Jensen et al., Mol. Cell 12, 1477 (2003).

9. M. Dam, K. Gerdes, J. Mol. Biol. 236, 1289 (1994).

10. F. van den Ent, J. Møller-Jensen, L. A. Amos, K. Gerdes, J. Lowe¨ , EMBO J. 21, 6935 (2002).

11. See supporting data on Science Online.

12. T. Mitchison, M. Kirschner, Nature 312, 237 (1984).

13. H. Wendel, P. Dancker, Biochim. Biophys. Acta 915, 199 (1987).

14. E. Nishida, H. Sakai, J. Biochem. (Tokyo) 93, 1011 (1983).

15. F. Oosawa, M. Kasai, J. Mol. Biol. 4, 10 (1962).

16. E. M. Mandelkow, G. Lange, A. Jagla, U. Spann, E. Mandelkow, EMBO J. 7, 357 (1988).

17. M. F. Carlier, R. Melki, D. Pantaloni, T. L. Hill, Y. Chen, Proc. Natl. Acad. Sci. U.S.A. 84, 5257 (1987).

18. E. C. Garner, C. S. Campbell, R. D. Mullins, data not shown.

19. C. Combeau, M. F. Carlier, J. Biol. Chem. 263, 17429 (1988).

20. L. Blanchoin, T. D. Pollard, Biochemistry 41, 597 (2002).

21. L. Romberg, T. J. Mitchison, Biochemistry 43, 282 (2004).

22. S. Vorobiev et al., Proc. Natl. Acad. Sci. U.S.A. 100,

5760 (2003).

23. D. Panda, H. P. Miller, L. Wilson, Biochemistry 41, 1609 (2002).

24. D. N. Drechsel, M. W. Kirschner, Curr. Biol. 4, 1053 (1994).

25. V. K. Vinson, E. M. De La Cruz, H. N. Higgs, T. D. Pollard, Biochemistry 37, 10871 (1998).

26. M. D. Welch, R. D. Mullins, Annu. Rev. Cell Dev. Biol. 18, 247 (2002).

27. S. H. Zigmond, Curr. Opin. Cell Biol. 16, 99 (2004).

28. M. Pring, M. Evangelista, C. Boone, C. Yang, S. H. Zigmond, Biochemistry 42, 486 (2003).

29. T. J. Mitchison, E. D. Salmon, Nature Cell Biol. 3, E17 (2001).

30. R. B. Jensen, K. Gerdes, J. Mol. Biol. 269, 505 (1997).

31. R. B. Jensen, K. Gerdes, EMBO J. 18, 4076 (1999).

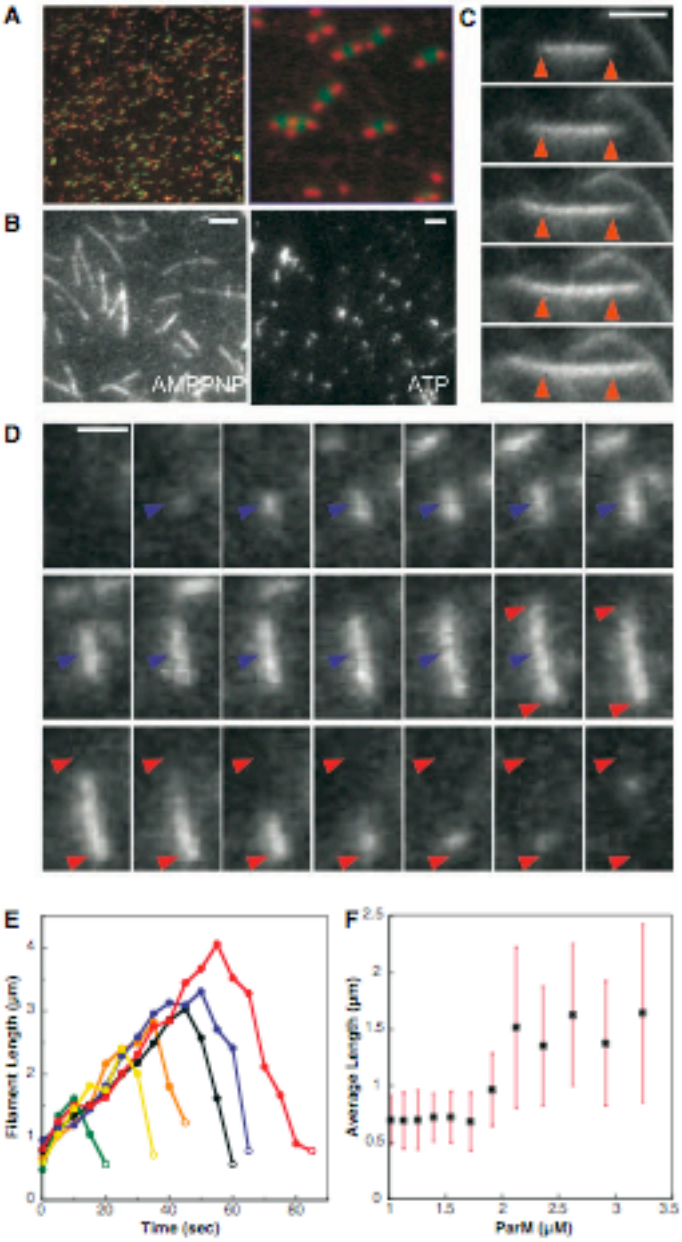


**Fig. 1.** Direct observation of bipolar elongation and dynamic instability. (A) ParM filaments elongate bidirectionally. On a poly-L-lysine–coated coverslip, 1 μl of 4.3 μM ParM labeled with Alexa 488 (green) was induced to polymerize by the addition of 0.2 μl of 100 mM AMP-PNP. After 30 s, we added 1 μl of 3.1 μM monomeric ParM labeled with Cy3 (red). After 1 min, the reaction was diluted with 20 μl of Buffer F [100 mM KCl, 30 mM tris-HCl (pH 7.5), 1 mM $MgCl_2$, and 1 mM dithiothreitol] and visualized by fluorescence microscopy. The left panel is an entire field visualized with a 100× objective. The right panel is a magnified region of the left. (B) Hydrolysis of ATP affects ParM filament length, as shown by TIRF microscopy of 2.7 μM Alexa 488–labeled ParM polymerized by addition of 10 mM AMP-PNP (left) or 10 mM ATP (right). Scale bars, 5 μm. (C) AMP-PNP ParM filaments elongate at equal rates from both ends, as shown by time-lapse TIRF microscopy of 2.7 μM ParM doped with 10% Alexa 488–labeled monomer polymerized by addition of 10 mM AMP-PNP. Orange arrowheads indicate the initial positions of the filament ends. Images are 50 s apart; scale bar, 5 μm. (D) In the presence of hydrolyzable ATP, ParM filaments polymerize with no detectable kinetic polarity and exhibit dynamic instability, as shown by time-lapse TIRF microscopy of 2.7 μM ParM doped with 10% Alexa 488–labeled monomer polymerized by addition of 10 mM ATP. The blue arrowhead designates the starting point of the filament; the red arrowheads show the endpoints before depolymerization. Images were collected 5 s apart; scale bar, 2 μm. (E) Length of filaments versus time for six representative filaments polymerized in ATP. The rates of ParM filament elongation and shortening are relatively constant from filament to filament, whereas the time spent in the elongation phase is variable. After switching from growth to shortening, every filament we observed disappeared completely. An open circle denotes that the given filament disappeared in the next frame. (F) ParM filaments appear above 2 μM and have a concentration-independent average length of 1.5 μm. Below 2 μM, most fluorescent structures observed are the size of diffraction-limited spots (0.75 μm) and probably do not represent bona fide filaments. Error bars represent SD.

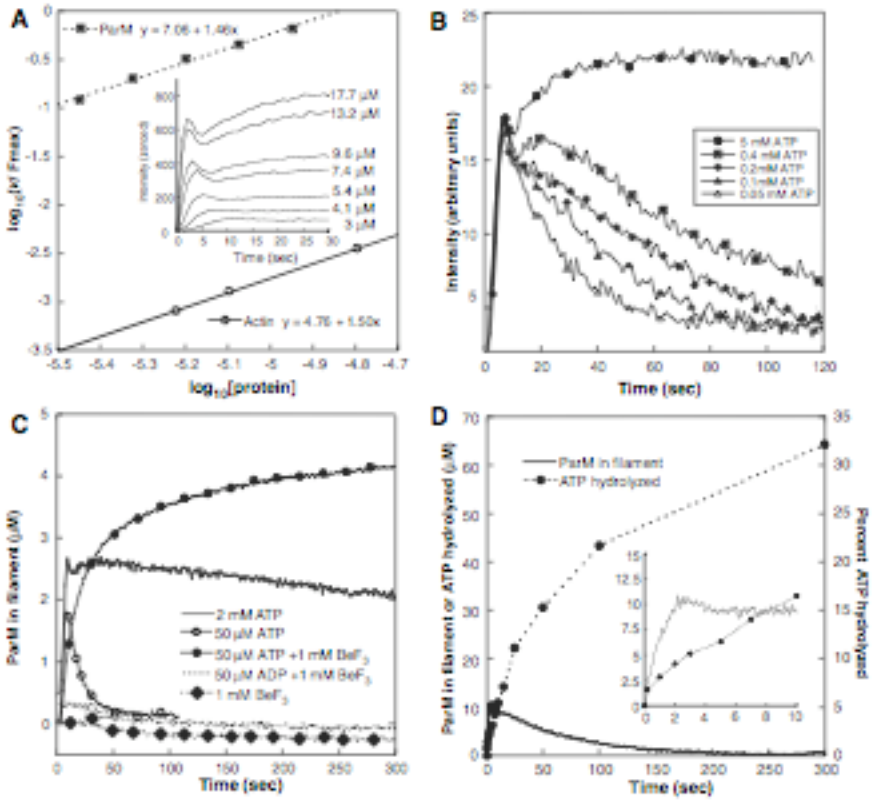


**Fig. 2.** Kinetics of ParM polymerization measured by FRET. (A) Determination of the nucleus size and relative nucleation rates of ParM and conventional actin filaments. FRET-labeled ParM (unlabeled ParM doped with 15% Cy3- and 15% Cy5-labeled monomer) was polymerized at varying concentrations by the addition of 5 mM ATP (inset). The maximal velocity of the polymerization signal was divided by the maximal fluorescence, and the log of this value was plotted against the log of the concentration of protein. The lines in the graph have a slope proportional to $(n - 1)$, where $n$ is the nucleus size, and the $x$ intercept is the relative nucleation rate ($k_{n+}$). This analysis shows that ParM and actin both elongate from nuclei composed of three monomers and that the spontaneous nucleation rate of ParM filaments is 300 times that of actin. (B) The lifetime of ParM filaments depends on ATP concentration. We used a rapid mixer to combine 5 μM FRET-labeled ParM with the indicated amount of ATP and monitored polymer content by FRET. (C) The phosphate analog $BeF_3$ stabilizes ParM filaments. We used a rapid mixer to combine 5 μM FRET-labeled ParM with ADP or ATP in the presence or absence of 1 mM $BeF_3$ and monitored polymer content by FRET. (D) ATP hydrolysis lags behind ParM polymerization. To monitor polymerization and ATP hydrolysis, we mixed 15 μM FRET-labeled ParM with 200 μM ATP doped with [γ-$^{32}$P]ATP. We monitored polymerization by mixing in a stopped-flow rapid mixer and monitoring FRET. We monitored ATP hydrolysis by mixing the samples in a quenched-flow rapid mixer and measuring the amount of radioactive phosphate released at various time points. Total polymer and cleaved phosphate are plotted on the same scale. (Inset) Expansion of the first 10 s of the plot.

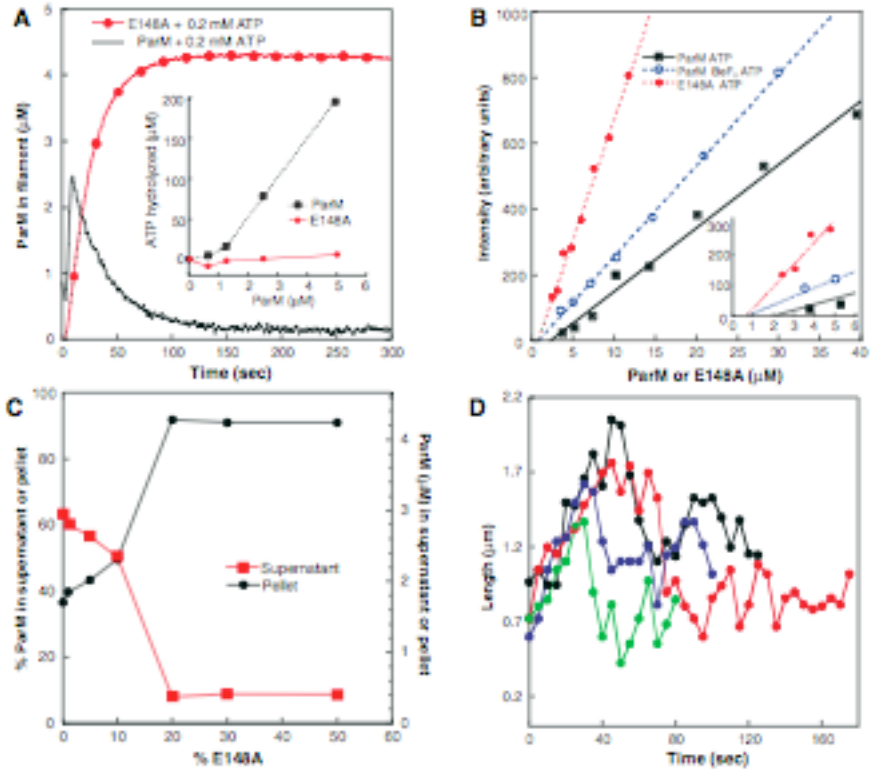


**Fig. 3.** Small amounts of nonhydrolyzing mutant ParM stabilize wild-type ParM filaments. (A) Mutating $Glu^{148}$ of ParM to alanine (E148A) abolishes hydrolysis of ATP and stabilizes ParM filaments. We measured polymerization kinetics by FRET using 5 μM FRET-labeled E148A or wild-type ParM. We used a stopped-flow rapid mixer to induce polymerization with 200 μM ATP. Inset: Bulk measurements of ATP hydrolysis by wild-type and E148A ParM. The indicated concentrations of wild-type or E148A ParM were combined with 1 mM ATP doped with [γ-$^{32}$P]ATP. The amount of cleaved radioactive phosphate was determined after 15 min. (B) The critical concentrations of the ATP (ATP + E148A) and ADP-Pi (ATP + $BeF_3$ + ParM) states are one-fourth the apparent ATP-ParM critical concentration. Serially diluted FRET-labeled wild-type ParM or E148A (95 μl in each case) was combined with 5 mM ATP or 5 mM ATP plus 1 mM $BeF_3$ within a cuvette. The unpolymerized signal was subtracted from the polymerized signal and plotted against the concentration of protein. The *x*-intercept values are taken as the critical concentrations. (C) Substoichiometric amounts of the hydrolysis-deficient ParM mutant stabilize ParM filaments. Cy3-labeled ParM (5.1 μM) was combined with Cy5-labeled E148A (5.1 μM) in the indicated ratios, polymerized with 10 mM ATP, and spun in an ultracentrifuge. Samples of supernatant and pellet were analyzed by SDS–polyacrylamide gel electrophoresis and quantitated with a fluorescent imager. Graph indicates the amounts of Cy3-ParM fluorescence. In the absence of E148A mutant ParM, the critical concentration of ParM is 2.7 μM. Addition of low concentrations of E148A ParM decreases the critical concentration. At 20% doping of the mutant, the critical concentration falls to ~0.5 μM—the critical concentration of E148A ParM alone. (D) Substoichiometric concentrations of E148A ParM promote rescue of depolymerizing ParM filaments. We plotted filament length versus time for four individual filaments (indicated by four colors) composed of 5% E148A and 95% wild-type ParM. Time zero corresponds to the initiation of a period of elongation. Unlike filaments composed entirely of wild-type ParM, the composite filaments oscillate in length and the switch from elongation to shortening does not always result in complete filament disassembly.

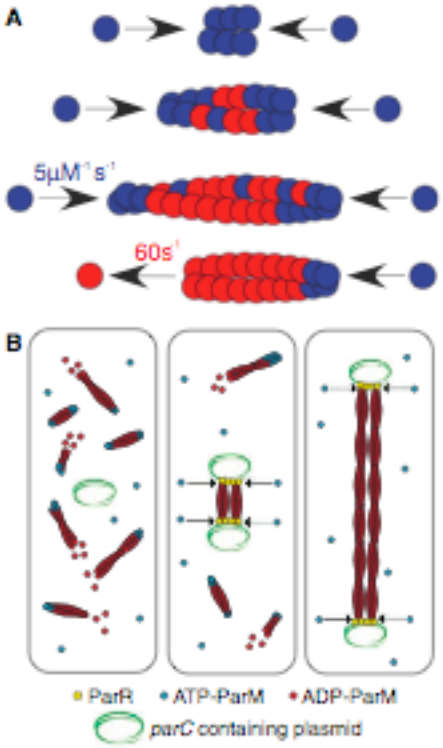


**Fig. 4.** Model for dynamic instability and in vivo function of ParM filaments. (A) Kinetic model for the dynamic instability of ParM. Once a nucleus is formed, the polymer elongates in a kinetically symmetrical manner. Polymerization induces ATP hydrolysis and ADP-bound monomers accumulate in the center of the filament. The filament remains stable as long as it maintains an ATP cap at both ends. When the cap at one end is lost, the polymer rapidly disassembles from that end. (B) Model for ParM-mediated plasmid segregation. ParM filaments spontaneously nucleate and elongate throughout the cell. Because of hydrolysis-induced dynamic instability, these polymers are unstable and they rapidly disassemble. Upon plasmid replication, two ParR-*parC* complexes form and are competent to capture and stabilize both ends of a set of ParM filaments. Through a mechanism of insertional polymerization at the ParM-ParR interface (arrows), the spindle elongates bidirectionally and pushes plasmids to the opposing ends of the cell.

# Chapter 3

This chapter contains the main conflict in the story of my thesis. Things started off well in the first two chapters, but now our protagonist needs a challenge to overcome for a truly satisfying story. The basis for this conflict lies in electron microscopy. Much of the work presented here is unpublished, which means no one will ever actually read about it.

After we determined that ParM is dynamically unstable, we wanted to see if the mechanism for the instability was similar to that of microtubules. By EM, rapidly depolymerizing microtubules have protofilaments that curl back. To see if ParM filaments have a similar type of rapid depolymerization following catastrophe, I used EM to look at negatively stained ParM. Initially, I simply compared ParM that was polymerized with ATP versus AMPPNP, as filaments polymerized with ATP will undergo catastrophe whereas those polymerized with AMPPNP will not. Unfortunately, there was no discernable difference between the two types of filaments (Figure 1A and 1B).

The lack of a visible difference between unstable and stabilized filaments could have been due to the fact that the majority of filaments polymerized with ATP would be in the polymerizing, rather than the depolymerizing state, in which case the ends would not be expected to look much different. Depolymerizing microtubules were observed by diluting them to induce catastrophe. In that way, all of the microtubules were shrinking when they were stained. Early attempts at this with ParM failed. After dilution, the filaments completely disappeared. Since ParM filaments are substantially shorter than

microtubules, by the time they were stained following dilution, they had completely depolymerized. To get around this, I raised the initial concentration of ParM above the ADP critical concentration of 100 micromolar. By starting with 120 micromolar ParM polymerized with ATP, I would expect to get much longer filaments that did not undergo catastrophe until dilution. In this way, I was able to observe filaments after dilution. By staining the filaments at different time points after dilution, I confirmed that the filaments were indeed depolymerizing. By five minutes post-dilution, the filaments were gone. However, there were still no visual changes in the structure of the filaments or their ends (Figure 1C). From this, I concluded that either ParM filaments do not depolymerize by the same protofilament pealing method of microtubules, or negative stain EM is not sufficient to observe the process. To date, no more light has been shed on the problem.

Another project that I was working on at the same time was trying to look at the whole structure of ParM, ParR, and parC by EM. Since negative stains do not work on DNA, I was forced to find another way of visualizing the complex. I chose rotary shadowing since it is commonly used for both DNA and protein, and was not as difficult a technique to learn as cryo. To do rotary shadowing, I first had to construct an atomizer. Samples must be mixed with glycerol and sprayed at fairly high velocity through a small whole in order to finely coat a piece of mica. The mica is then shadowed with platinum and coated with carbon. The carbon is floated off of the mica onto water and put on a copper grid. My first attempts at constructing an atomizer using a turkey baster were too inconsistent. Dr. Mullins lent me his old air brush, which, with only a few modifications, turned into a fine atomizer.

DNA stood up very well to the atomization process, and was seen clearly by rotary shadowing (Figure 2A and 2B). ParM filaments on their own fell apart during the atomization. Even filaments stabilized with AMPPNP disintegrated when sprayed, and no filaments were seen by shadowing. Crosslinking the filaments with a combination of gluteraldehyde and lysine protected filament integrity through the process (Figure 2C). To my dismay, this same procedure completely destroyed the DNA. Both gluteraldehyde and lysine were necessary to visualize filaments, and both were also required to destroy the DNA. At this point, I got very frustrated. Since my other line of investigation (see Chapter 4) was showing more progress, I decided to focus on that.

One positive thing did come out of my EM studies. A while later, Ethan Garner was working on a system to reconstitute the par operon using parC attached to beads. Since I no longer needed to visualize the DNA directly, I could look at the structures by negative stain. Early attempt were fairly successful, showing massive bundles of filaments in between two beads (Figure 3A). What I really wanted was to determine if a single ParM filament could be attached to a bead at each end. Our theory at the time was that each end of the ParM filament needed to be stabilized by a ParR/parC complex in order to function in segregation. This was an unpopular theory, as detailed structural work indicated that ParM filaments have two structurally distinct ends. It seemed unlikely that different structures would be able to interact with the ParR/parC complex in exactly the same way. As it turned out, they do. I was able to obtain some images of single filaments that spanned from one bead to another (Figure 3B). Although we still can't explain exactly how these interaction occur with distinct binding surfaces, we know that they do.

Figure 1

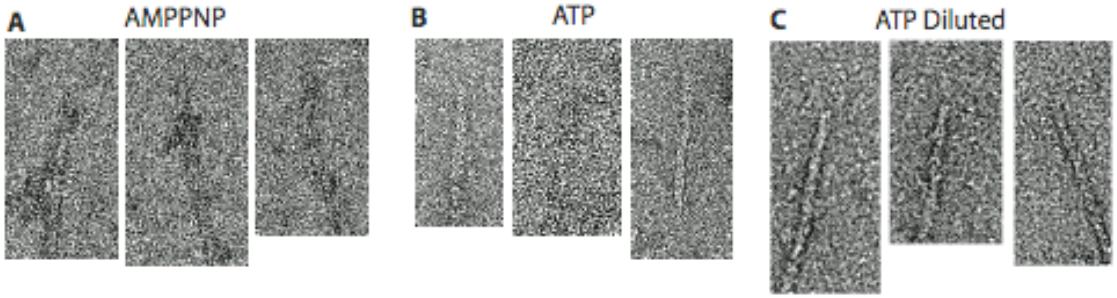

Figure 2

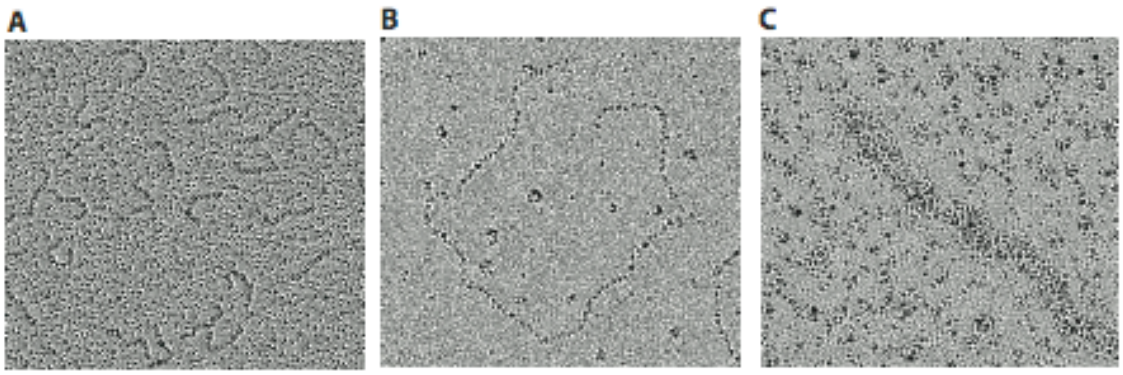

Figure 3

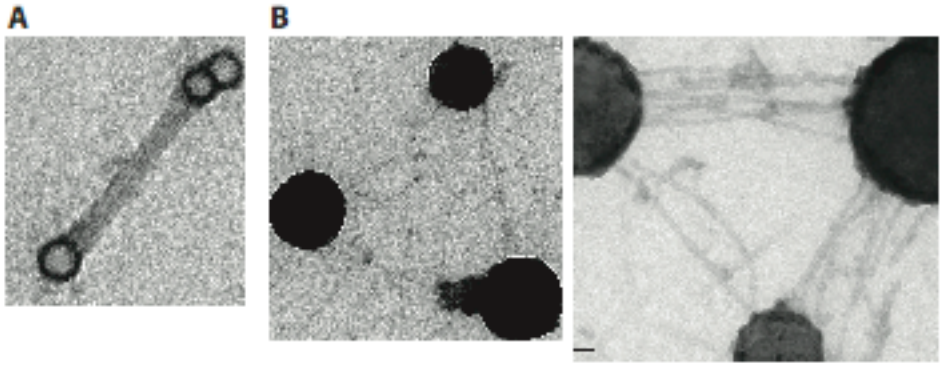

# Chapter 4

## Introduction

Transmission of genetic information from one generation to the next requires efficient partitioning of DNA molecules between daughter cells. Eukaryotic DNA segregation relies on construction of a complex mitotic spindle that finds and aligns sister chromatids and then moves them to opposite sides of the cell division plane (Inoue, 1953). This process is conserved across eukaryotic phyla, and the molecular mechanisms driving it have been extensively studied. In contrast, the mechanisms driving prokaryotic chromosome segregation are still poorly understood.

The best understood example of bacterial DNA segregation is the partitioning of low-copy plasmids. Plasmids are circular pieces of extrachromosomal DNA that often contribute to virulence and antibiotic resistance in pathogenic bacteria. Large, low-copy plasmids encode simple segregation systems to ensure that at least one copy of the plasmid ends up on each side of the cell division plane and is inherited by each daughter. The majority of these segregation systems fall into one of two classes: Type I or Type II. The segregation operons of both classes are composed of three components: (i) a centromeric DNA sequence, and genes encoding: (ii) a DNA binding protein, and (iii) an ATPase. The classes are distinguished primarily by the structure of the ATPase component (For review, see Ebersbach and Gerdes, 2005). Type I segregation operons encode a deviant Walker-box ATPase (ParA) while type II segregation operons encode an actin-like ATPase (ParM).

The most thoroughly characterized plasmid segregation system is the Type II mechanism that drives segregation of the R1 multi-drug resistance plasmid isolated from *E. coli* (Gerdes and Molin, 1986). The R1 *par* operon encodes a ParM that forms actin-like filaments in the presence of ATP (Moller-Jensen et al., 2002) and a DNA binding protein, ParR, that binds a series of 10 direct sequence repeats in the centromeric *parC* DNA (Jensen et al., 1998). By total internal fluorescence microscopy, purified ParM forms filaments that are dynamically unstable and polymerize bidirectionally (Garner et al., 2004). The ParR/*parC* protein-DNA complex forms a structure analogous to a eukaryotic kinetochore that binds to either end of a ParM filament and suppresses dynamic instability. Insertional polymerization at the plasmid/filament interface generates force capable of segregating *parC*-coated beads. Based on these data, it has been proposed that two plasmids can capture opposite ends of the same ParM filament and that polymerization pushes the plasmids apart (Garner et al., 2007).

ParM-dependent DNA segregation has been reconstituted and studied *in vitro* but the dynamics of plasmid segregation *in vivo* are unknown. To date, microscopic studies of type II plasmid segregation in bacteria have been based on either fixed cells or static images of live cells (Jensen and Gerdes, 1999; Moller-Jensen et al., 2003; Weitao et al., 2000). Time-lapse light microscopy of living cells has provided key insights into the structure and function of the mitotic spindle in eukaryotes (Inoue, 1953; Rieder et al., 1986). In this study, we use time-lapse imaging of fluorescently labeled ParM filaments and plasmids to follow the *in vivo* dynamics of ParM filament assembly and plasmid segregation. We find that segregation driven by the *par* operon is a highly dynamic process. Individual *par*-containing plasmids undergo diffusive motions that are

significantly faster than those of control plasmids lacking the par-operon. Pairs of plasmids are rapidly pushed toward the poles of the cell by elongating ParM filaments. Once they reach the poles, the ParM filaments disassemble and the plasmids resume diffusive motion. Remarkably, multiple plasmids in the same cell can interact multiple times in a single cell cycle and undergo multiple rounds of segregation.

**Results**

We used time-lapsed fluorescence microscopy to compare plasmid dynamics in the absence and presence of the *par* operon. To visualize plasmids, we used a system first developed by Straight et. al (Straight et al., 1996) in which LacI-GFP is bound to a tandem array of *lacO* sites integrated into the plasmid. We co-transformed *E. coli* cells with a low-copy, mini-F plasmid containing the *par* operon from plasmid R1 and a series of 256 *lacO* repeats together with a plasmid expressing LacI-GFP. Cotransformed cells contained bright fluorescent foci. Control cells transformed with one plasmid or the other by itself contained no fluorescent foci, indicating that both LacI-GFP and the *lacO* repeats are necessary to generate fluorescent foci. We determined plasmid positions at every time point and plotted mean squared displacement (MSD) as a function of time. As a control, we looked at plasmids in fixed cells to show that noise and stage drift do not have a significant effect on our MSD measurements (Figure 1A). When analyzed on short time scales (<60 seconds), plasmids lacking the *par* operon undergo very slow, diffusive motions, with an average diffusion coefficient of $5 \times 10^{-5}$ $\mu m^2$/sec (Figure 1A and 1B). The rate is significantly less than that for GFP alone (8 $\mu m^2$/sec) (Elowitz et al., 1999) or GFP-labeled mRNA ($10^{-3}$ to $10^{-2}$ $\mu m^2$/sec) (Golding and Cox, 2006).

Additionally, at time intervals less than 200 seconds, the MSD increases linearly with time, meaning that the movements are neither directed nor constrained. At longer time scales (>1000 seconds) the mean squared displacement of the labeled plasmids departs from linearity and eventually plateaus, indicating that the diffusive motions of the plasmids are confined within a small volume. The average confinement radius is 275nm, smaller than the dimensions of the bacterium (Figure 1C), implying that the plasmids are confined to subcellular compartments in which they are free to diffuse, but from which they rarely escape. These cytoplasmic pockets can be viewed directly by projecting the maximum intensities of all of the pixels on all of the images of a time lapse sequence onto a single image (Figure 1D).

The maximum number of foci observed in a given cell over a time course ranged from zero to four (Supplemental Table 2). This is in agreement with estimates by Collins and Pritchard (Collins and Pritchard, 1973) that the F plasmid is present at approximately one copy per chromosome equivalent. We next analyzed the motion of plasmids containing the *par* operon. In cells with only a single fluorescent spot, the plasmid also undergoes apparently diffusive motion (Figure 1E), but with a significantly higher diffusion coefficient ($4 \times 10^{-4}$ $\mu m^2$/sec) and confinement radius (420 nm), indicating that the *par* operon increases the mobility of individual plasmids (Figure 1A-C). In cells containing multiple foci the labeled plasmids frequently converge to form clusters, as observed in previous studies (Ebersbach et al., 2005; Li and Austin, 2002; Pogliano et al., 2001). The number of fluorescent foci in an individual image, therefore, does not necessarily reflect the total number of plasmids present in a cell. For this reason, we classify cells based on the maximum number of foci observed over the entire acquisition

time. Cells with two foci exhibit a much different behavior from those containing only a single focus (Figure 1F). Both foci move randomly and independently until they come into close proximity and merge into a single fluorescent spot. The plasmids then move together as a single unit for a few seconds, until they split and move rapidly in opposite directions, one bright spot moving to each pole of the cell. After remaining immobilized at the poles for several seconds, the plasmids begin to move diffusively again and slowly migrate around the cell until they encounter each other once more and repeat the entire process. In cells with three foci, the plasmids often develop a stable oscillatory pattern in which one fluorescent spot is maintained at each pole while a third spot undergoes repeated pole-to-pole movements (Figure 1G). We observe this "ping-pong" behavior only in cells with three plasmid foci. The pole-to-pole movements take 10 to 30 seconds and always alternate direction. This oscillatory behavior maintains at least one plasmid at each end at all times. Plasmids undergoing rapid pole-to-pole motion occasionally pause near the center of the cell before continuing to the pole (Figure 1G second translocation). The time between pole-to-pole movements is highly variable, ranging from 0 to 150 seconds (59 +/- 37 sec, n = 30). Zero second dwell times indicate that plasmids switched directions before traveling all the way to the other pole. After merging, a cluster of two foci often moves slightly away from the pole immediately before segregation (Figure 1F first segregation, Figure 1G first and third segregations). Cells with four foci are rare, and the frequent clustering and unclustering of the plasmids make generalizations about their behavior difficult (Supplemental Figure 3). Although the dynamics in this case are complicated, one plasmid is almost always located near each pole.

For plasmid inheritance, the most important DNA segregation events are those that occur immediately prior to cell division. For this reason we wanted to see if plasmid behavior changed during septation. In actively dividing cells containing three plasmid foci, plasmids continue to oscillate from pole to pole. We observed cells in which a plasmid moved through a narrowing septum and then attempted to move back but failed to pass the site of septation, presumably blocked by septum closure (Supplemental Figure 2A).

By immunofluorescence, Moller-Jensen et al. observed ParM filaments in approximately 40 percent of cells containing plasmids with the R1 *par* operon. These filaments often ran from pole to pole and were associated with fluorescently labeled plasmids (Moller-Jensen et al., 2003; Moller-Jensen et al., 2002). To better understand the mechanism behind the observed plasmid dynamics we used time-lapse fluorescence microscopy to study assembly of ParM filaments *in vivo*. To monitor ParM dynamics, we used a GFP-ParM fusion protein expressed in cells with a *par*-containing plasmid. By having the unlabeled ParM expressed from the wildtype operon present, we minimize any negative effects of the GFP fusion. This technique has been successful for visualizing actin and other actin related proteins (Gitai et al., 2004; Westphal et al., 1997). Overexpression of GFP-ParM produced bright, stable filaments in all cells observed (data not shown). Filaments appeared regardless of the presence of ParR and *parC*. When we turned off expression of GFP-ParM and diluted the fluorescent protein by allowing cells to multiply for 4 to 6 generations, we began to see dynamic filaments (Figure 2). In contrast to the bundles seen when GFP-ParM was overexpressed, we observed these filaments only in the presence of the additional plasmid containing the *par* operon. These

structures, which we call "spindles" by analogy with the eukaryotic DNA segregation machinery, elongate for up to a minute before switching from elongation to rapid shortening. This behavior is very similar to the dynamic instability seen *in vitro* with purified ParM (Garner et al., 2004). The spindles never last longer than 3 minutes, indicating that stabilization against catastrophe by the ParR/*parC* complex is limited *in vivo*. Consistent with our observations of plasmid movement, elongation of ParM spindles sometimes slows when one end nears the center of the cell (Figure 2A and 2B, purple arrows). More rarely, we observe pauses in shortening (Figure 2A and 2B, yellow arrows). We never observed a switch from shortening to elongation.

How do ParM filaments find the long axis of the host cell? In our time-lapse movies we note that ParM spindles do not always initially align with the long axis (Figure 2C). In cases where spindles originally elongate orthogonal to the long axis, they quickly make contact with the sides of the cell. Continued elongation then proceeds together with alignment along the long axis. This result demonstrates that the initial spindle orientation is not predetermined by a cellular landmark, and that alignment with the long axis is probably driven by elongation of the spindle itself.

In fixed cells ParM spindles are frequently curved (Moller-Jensen et al., 2002). This could result from filament buckling caused by continued polymerization against both poles of the bacterium. However, spindles also frequently show curvature as they elongate across the cell (Figure 2A last 4 frames and Figure 2E), suggesting that bending of the filaments often results from interaction with intracellular obstacles such as the nucleoid.

One important question is whether ParM spindles are composed of one filament or bundles of multiple filaments. Evidence that ParM spindles are filament bundles comes from the fact that spindles do not always depolymerize in a single step. In rare cases, spindles first show a significant overall decrease in fluorescence before completely depolymerizing (Figure 2D, Supplemental Figure 1). Kymograph analysis of these spindles shows that the decrease in fluorescence intensity is directional, moving from one end of the spindle to the other, and proceeds at the same rate as catastrophic depolymerzation. The remaining spindle continues to elongate until it, too deplymerizes. Although these data indicates that at least some spindles contain multiple filaments, we cannot rule out that these spindles are generated by clusters of linked plasmid rather than individual plasmid pairs.

To determine the directionality of polymerization, we photobleached a small section of a spindle to create a fiducial mark. Both ends of the spindle polymerize away from the mark at similar rates, indicating that, similar to *in vitro* reconstituted spindles (Garner et al., 2007), polymerization occurs simultaneously at both ends of a spindle. Also, when one end of the filament abuts the side of the cell, the bleached mark migrates in the opposite direction at a rate half that of the full spindle, indicating that polymerization against a barrier can drive the entire spindle through the cytoplasm (Figure 2E).

To determine the connection between plasmid movement and ParM dynamics, we expressed mCherry-ParM in cells containing labeled plasmids and imaged both labels. In cells that contain both ParM filaments and plasmid foci (n = 178), spindles always colocalized with the plasmid (Figure 3). In all cases where we observed pairs of plasmids

moving rapidly in opposite directions, the plasmid pairs were separated by an elongating ParM spindle (Figure 3A). After plasmids reach the poles and stop moving, the associated spindles rapidly depolymerize. Plasmids move apart on elongating ParM spindles but we never observed plasmids moving on shortening spindles.

Single plasmid foci are also associated with increased mCherry fluorescence. The ParM fluorescence extends beyond the fluorescence of the plasmids, suggesting that short filaments extend from the plasmids (Figure 3B). These filaments are generally shorter, dimmer, and more dynamic than those that form the spindles associated with pairs of plasmid foci (Figures 3C and 2C). One end of these filaments appears to be bound and stabilized by the ParR/*parC* complex, while the other is presumably "searching" for additional plasmids. These structures are similar to ParM asters that form around isolated, *parC*-coated beads *in vitro* (Garner et al., 2007), and probably explains the faster diffusive motions we observed for single plasmids containing the *par* operon. Thus, it appears that type II *par* operons evolved to enable plasmids to both search for partners and to be efficiently captured by other searching plasmids. That is, they play the role of both spindle pole and kinetochore.

We next measured the rates of spindle elongation and disassembly as well as the rate at which plasmids move apart from each other (Table 1). The rates of spindle polymerization and plasmid segregation are nearly identical. This rate is also close to the previously measured rates of polymerization of ParM *in vitro*. This result has two important implications. First, polymerization at both ends of ParM filaments powers plasmid segregation. Previous work has shown that ParM filaments polymerize equally from each end both in isolation (Garner et al., 2004) and when associated with the

ParR/*parC* complex (Garner et al., 2007). The *in vitro* rate in Table 1 is for both ends combined. Since plasmids move at this rate, they are being propelled by polymerization at both ends of the spindle, as confirmed by photobleaching experiments (Figure 2E). The second implication of these measurements is that the amount of monomer in the bacterium is at the steady state of 2.3 $\mu$M. Previous estimates for the total concentration of ParM protein expressed in *E. coli* are around 15μM (Moller-Jensen et al., 2002). If this were the concentration of free, monomeric ParM, we would expect an initial rate of polymerization 6 to 7 times greater than that observed. Therefore, we suggest that there is ParM polymer present in cells even when spindles are not visible. This result is in agreement with ParM having a very low nucleation barrier (Garner et al., 2004). Most likely this polymer is not seen because it is in the form of short, rapidly diffusing filaments distributed throughout the cytoplasm. The simplest explanation for why the spindles can be seen over this background of dynamic polymer is that they are bundles of multiple filaments, making them brighter than single filaments. Alternatively, association with a 19 megadalton plasmid may decrease the diffusion of the filaments such that they are less likely to move during image acquisition.

The depolymerization rate of ParM spindles is variable, but generally faster than that measured for single ParM filaments *in vitro* (Table 1). This may be explained by the fact that the ParR/*parC* complex prevents catastrophe when filament polymerization stalls (Figure 2A 50-80 seconds), allowing hydrolysis of more ATP in the filaments. When catastrophe eventually occurs, depolymerization proceeds more quickly because more of the polymer is in the unstable, ADP-bound form.

**Discussion**

This study provides three basic insights into type II plasmid segregation. First, ParM filaments are dynamically unstable *in vivo*. When both plasmid-bound ends of a bipolar ParM spindle reach the poles, elongation stalls. After a few seconds, the spindle either breaks or dissociates from one of the plasmids, becomes unstable, and falls apart. We observed this directly by imaging fluorescent ParM spindles and indirectly by observing the behavior of the plasmids. After segregation, plasmids do not remain fixed at the poles, indicating that the spindle that pinned them to the poles has disassembled and that they are not anchored to polar landmarks in the host cell. Second, when only one plasmid is present, filaments are bound and stabilized at only one end. The other, unstable end is presumably competent to interact with a second plasmid and may mediate search-and-capture as observed *in vitro* (Garner, 2007). These monovalent attachments also drive plasmids in a diffusive random walk through the cytoplasm at rates greater than diffusion in the absence of the *par* operon. This may further increase the efficiency of the search for sister plasmids. Third, *in vivo*, ParM spindles can be composed of multiple filaments. Spindles reconstituted *in vitro* contain many filaments, but this is at least partially the result of having many copies of the *parC* DNA immobilized on a single bead (Garner et al., 2007). These results suggest that either a single ParR/*par*C complex may interact with multiple ParM filaments, or multiple pairs of plasmids can cooperate to form a spindle.

The results from this study also confirm many conclusions based on *in vitro* experiments. Most notably, the behavior of filaments in cells is highly reminiscent of the dynamic instability of filaments observed *in vitro* (Garner et al., 2004). In both cases,

filaments were short-lived and recovery from catastrophic depolymerization is not observed. Additionally, the binding of plasmids to each end of a spindle as it elongates is reminiscent of the *in vitro* reconstitution of the system using polystyrene beads (Garner et al., 2007). The rates of polymerization at steady-state for single ParM filaments or ParR/*parC* associated filament bundles *in vitro* were very similar to those measured *in vivo*. The similarities between the *in vivo* observations and the reconstitution with purified components strongly suggest that host factors are not required for segregation and the conditions used for the *in vitro* experiments more or less mimic cellular conditions.

An important implication of the frequent directional movements of *par* containing plasmids is that, unlike previously observed mechanisms of DNA segregation, type II plasmid segregation is a dynamic process that continues throughout the cell cycle. Plasmids are biased towards the ends of a cell and generally away from the plane of division rather than being immobilized at the poles. The apparent inefficiency of this system may reflect the small number of components used to construct the segregation machinery and the fact that it has not evolved to use host cell factors for anchoring to the poles. In fact the broad host range of *par*-containing plasmids may make it impractical to rely on any specific host cell factor. The dynamics of segregation provide a potential mechanism for correcting mistakes. If one attempt at segregation fails and both plasmids end up on the same side of the division plane, the system can try again. Our observation that segregation is not coordinated with the cell cycle agrees with previous observations that R1 plasmid replication is uncoupled from chromosome replication (Gustafsson et al., 1978).

Our model for *in vivo* plasmid segregation (Figure 4) highlights two important and unanswered questions regarding the interaction between ParM filaments and the ParR/*parC* complex. First, if the ParM binding sites on the ParR/*parC* complex are occupied by the ends of searching filaments, how can they capture the ends of filaments attached to a different plasmid? We propose two possibilities. (1) Free ends of monovalently attached filaments could anneal, creating a single stabilized filament. (2) At a given time, only a fraction of filament binding sites may be occupied by mono-attached filaments, leaving the rest available for capture. Another question concerning the filament/plasmid interaction is: how does a single complex bind and stabilize the two structurally distinct filament ends? By electron microscopy, ParM filaments are composed of two parallel and polarized protofilaments, which create two completely different ends (van den Ent, 2002; Orlova, 2007). We previously showed that both ends of an individual ParM filament can bind to the ParR/*parC* complex (Garner et al., 2007). From a structural perspective, it is difficult to imagine the ParR/*parC* complex interacting with two different surfaces in the exact same manner. Either the ParR/parC complex contains two distinct ParM binding sites, one specific for each end, or most of the molecular contacts are with the side of the filaments.

**Materials and Methods**

Construction of bacterial strains and plasmids:

Splicing by overlapping extension (SOE) PCR was used to make a GFP fusion to the ParM gene from plasmid R1-19 and inserted into the NDE1 and BamH1 sites of pET11a

(New England Biolabs) to create pCC110. pCC121 was made by using SOE PCR to fuse mCherry to ParM and inserting into the XBA1 and SAL1 sites of the CRIM vector pTB97 (containing a phage HK022 att site). This was then inserted into the *E. coli* strain TB20 (MG1655 Δlac) and checked for single integrants as previously described (Haldimann and Wanner 2001) to create the strain CC1.

Growth and Expression:

All cultures were grown in LB media with the appropriate antibiotics at the following concentrations: 100 ng/mL ampicillin, 20 ng/mL kanamycin, 68 ng/mL chloramphenicol. For expression of GFP-ParM, pCC110 was transformed into BL21 cells with pLysS (Studier et al., 1990) and pRBJ460 (Jensen and Gerdes, 1999). pLysS is required to turn off the expression of GFP-ParM. Cells were grown to an OD600 of 0.5 and induced with 3mM IPTG for 1.5 hours. Cells were then centrifuged, resuspended in the same volume of fresh LB, and diluted 1:100 in LB with kanamycin and chloramphenicol. After 2 hours of outgrowth, samples were removed for microscopy. For plasmid visualization, pRBJ460 or pRBJ461 (Jensen and Gerdes, 1999) were co-transformed with pJMJ178 (Moller-Jensen et al., 2003) into the strain MG1655. Plasmids pRBJ460 and pRBJ461 are mini-F plasmids to which 256 *lacO* repeats and a portion of the R1 plasmid have been added. pRBJ460 contains the R1 *par* operon and pRBJ461 contains the *hok*/*sok* system. For dual visualization of plasmids and filaments, pRBJ460 and pJMJ178 were co-transformed into CC1. Cultures were grown overnight in chloramphenicol and kanamycin. For cell fixation, 2x fixing solution (60mM phosphate pH 7.0, 4.8% paraformaldehyde, .08% gluteraldehyde) was mixed 1:1 with a

bacterial culture and incubated and room temperature for 10 minutes and then at 4 degrees Celsius for at least an hour. For Microscopy, 1.5 $\mu$L of cells were placed on top of 70 $\mu$L M9 media (plus .2% glucose) agar (1.5%) pads and sealed with a 1:1:1 (by weight) mixture of petroleum jelly (Vasaline), lanalin, and parafin.

Microscopy:

Three microscopes were used in this study. The first is a Nikon TU300 equipped with an ORCA 2 ER CCD and has been described previously (Garner et al., 2007). The primary microscope that was used is a Nikon TE 2000 with a Perfect Focus module, equipped with an Andor Ixon CCD and an ORCA ER camera. The objective used was a Nikon Apo TIRF 100x 1.49 NA oil immersion. For some experiments, an objective heater (Bioptechs) and air stream stage incubator (Nevtek) were used to heat the samples to 37 degrees Celsius. Images were acquired with the open source $\mu$Manager software version 1.0.60 (micro-manager.org). Photobleaching experiments were performed with a Zeiss LSM510 confocal microscope.

Image Analysis:

ImageJ (NIH) was used for length measurements, contrast adjustment, image rotation and making kymographs. For diffusion rates, plasmid tracking was done with MATLAB (MathWorks). Peaks in fluorescence were identified using the 'pkfnd' module of Eric Dufresne (Yale). The addition of a Gaussian fitting module to obtain sub-pixel resolution did not alter the results, and was not included in the final build. To determine

which foci were considered to be from the same plasmid from frame to frame, the 'track' module by John C. Crocker (University of Chicago) was implemented. Mean square displacements for each track were calculated by averaging the squares of the displacement for all pairs of time points for each time interval.

**References**

Collins, J., and R.H. Pritchard. 1973. Relationship between chromosome replication and F'lac episome replication in Escherichia coli. *J Mol Biol*. 78:143-55.

Ebersbach, G., and K. Gerdes. 2005. Plasmid segregation mechanisms. *Annu Rev Genet*. 39:453-79.

Ebersbach, G., D.J. Sherratt, and K. Gerdes. 2005. Partition-associated incompatibility caused by random assortment of pure plasmid clusters. *Mol Microbiol*. 56:1430-40.

Elowitz, M.B., M.G. Surette, P.E. Wolf, J.B. Stock, and S. Leibler. 1999. Protein mobility in the cytoplasm of Escherichia coli. *J Bacteriol*. 181:197-203.

Garner, E.C., C.S. Campbell, and R.D. Mullins. 2004. Dynamic instability in a DNA-segregating prokaryotic actin homolog. *Science*. 306:1021-5.

Garner, E.C., C.S. Campbell, D.B. Weibel, and R.D. Mullins. 2007. Reconstitution of DNA segregation driven by assembly of a prokaryotic actin homolog. *Science*. 315:1270-4.

Gerdes, K., and S. Molin. 1986. Partitioning of plasmid R1. Structural and functional analysis of the parA locus. *J Mol Biol*. 190:269-79.

Gitai, Z., N. Dye, and L. Shapiro. 2004. An actin-like gene can determine cell polarity in bacteria. *Proc Natl Acad Sci U S A*. 101:8643-8.

Golding, I., and E.C. Cox. 2006. Physical nature of bacterial cytoplasm. *Phys Rev Lett*. 96:098102.

Gustafsson, P., K. Nordstrom, and J.W. Perram. 1978. Selection and timing of replication of plasmids R1drd-19 and F'lac in Escherichia coli. *Plasmid*. 1:187-203.

Inoue, S. 1953. [Polarization optical studies of the mitotic spindle. I. The demonstration of spindle fibers in living cells.]. *Chromosoma*. 5:487-500.

Jensen, R.B., and K. Gerdes. 1999. Mechanism of DNA segregation in prokaryotes: ParM partitioning protein of plasmid R1 co-localizes with its replicon during the cell cycle. *Embo J*. 18:4076-84.

Jensen, R.B., R. Lurz, and K. Gerdes. 1998. Mechanism of DNA segregation in prokaryotes: replicon pairing by parC of plasmid R1. *Proc Natl Acad Sci U S A*. 95:8550-5.

Li, Y., and S. Austin. 2002. The P1 plasmid is segregated to daughter cells by a 'capture and ejection' mechanism coordinated with Escherichia coli cell division. *Mol Microbiol*. 46:63-74.

Moller-Jensen, J., J. Borch, M. Dam, R.B. Jensen, P. Roepstorff, and K. Gerdes. 2003. Bacterial mitosis: ParM of plasmid R1 moves plasmid DNA by an actin-like insertional polymerization mechanism. *Mol Cell*. 12:1477-87.

Moller-Jensen, J., R.B. Jensen, J. Lowe, and K. Gerdes. 2002. Prokaryotic DNA segregation by an actin-like filament. *Embo J*. 21:3119-27.

Orlova, A., E.C. Garner, V. E. Galkin, J. Heuser, R. D. Mullins, and E. H. Egelman. 2007. *Nat Struct Mol Biol*. In press.

Pogliano, J., T.Q. Ho, Z. Zhong, and D.R. Helinski. 2001. Multicopy plasmids are clustered and localized in Escherichia coli. *Proc Natl Acad Sci U S A*. 98:4486-91.

Rieder, C.L., E.A. Davison, L.C. Jensen, L. Cassimeris, and E.D. Salmon. 1986. Oscillatory movements of monooriented chromosomes and their position relative to the spindle pole result from the ejection properties of the aster and half-spindle. *J Cell Biol*. 103:581-91.

Straight, A.F., A.S. Belmont, C.C. Robinett, and A.W. Murray. 1996. GFP tagging of budding yeast chromosomes reveals that protein-protein interactions can mediate sister chromatid cohesion. *Curr Biol*. 6:1599-608.

Studier, F.W., A.H. Rosenberg, J.J. Dunn, and J.W. Dubendorff. 1990. Use of T7 RNA polymerase to direct expression of cloned genes. *Methods Enzymol*. 185:60-89.

van den Ent, F., J. Moller-Jensen, L.A. Amos, K. Gerdes, and J. Lowe. 2002. F-actin-like filaments formed by plasmid segregation protein ParM. *Embo J*. 21:6935-43.

Weitao, T., S. Dasgupta, and K. Nordstrom. 2000. Plasmid R1 is present as clusters in the cells of Escherichia coli. *Plasmid*. 43:200-4.

Westphal, M., A. Jungbluth, M. Heidecker, B. Muhlbauer, C. Heizer, J.M. Schwartz, G. Marriott, and G. Gerisch. 1997. Microfilament dynamics during cell movement and chemotaxis monitored using a GFP-actin fusion protein. *Curr Biol*. 7:176-83.

Figure 1

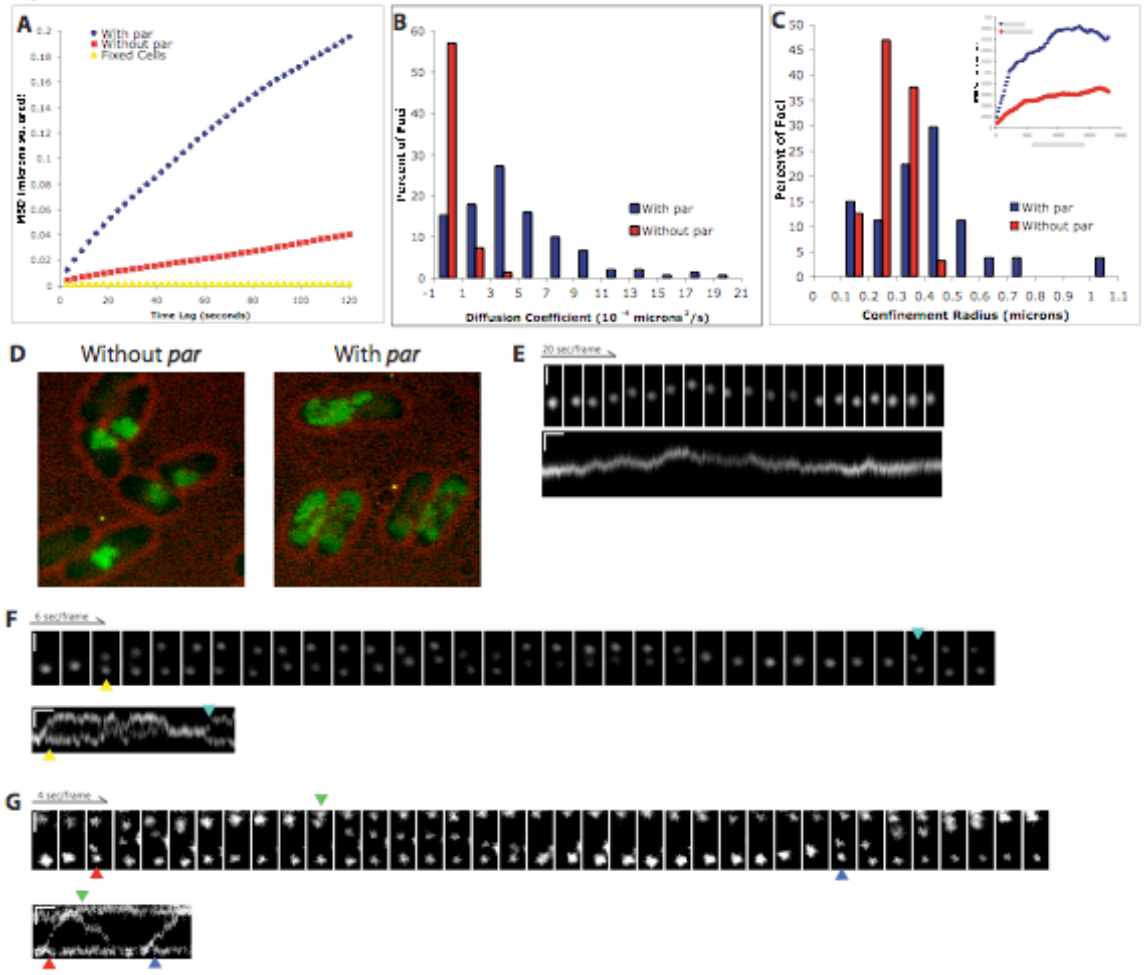


Figure 1.

*Par*-containing plasmids undergo both rapid, directional and slow, diffusive movements. Arrows point to the initiation of segregation events. The colors of the arrows are coordinated between image montages and kymographs.

(**A**) Mean squared displacement versus time lag for plasmids with the *par* operon (pRBJ460, average of 151 foci) and those that do not contain the *par* operon (pRBJ461, average of 99 foci).

(**B**) Distribution of diffusion coefficients for plasmids with and without the *par* operon. The diffusion coefficient was measured by taking the slope of individual MSD versus time lag traces and dividing by 4 (for the 2 degrees of freedom).

(**C**) Distribution of Confinement radii for plasmids with (n = 27) and without (n = 32) the *par* operon. The plateau of each MSD was estimated by averaging the 1800 through 2000 second time points. The square root of the plateau value was then taken to get the confinement radius for each trace. Inset: Representative traces of MSD versus time lag for the longer time intervals used to estimate confinement sizes.

(**D**) Maximum intensity projection of plasmids with and without the *par* operon over the course of a 2000 second time series.

(**E**) Cell with a single *par*-containing plasmid focus exhibiting diffusive movements.

(**F**) Cell with two *par*-containing plasmid foci displaying mostly diffusive movements with occasional periods of rapid segregation.

(**G**) Example of the rapid pole-to-pole movements seen in cells with three *par*-containing plasmid foci.

Vertical scale bars are 1$\mu$m. Horizontal scale bars in kymographs are 20 seconds. All images were contrast adjusted for clarity and rotated for ease of presentation.

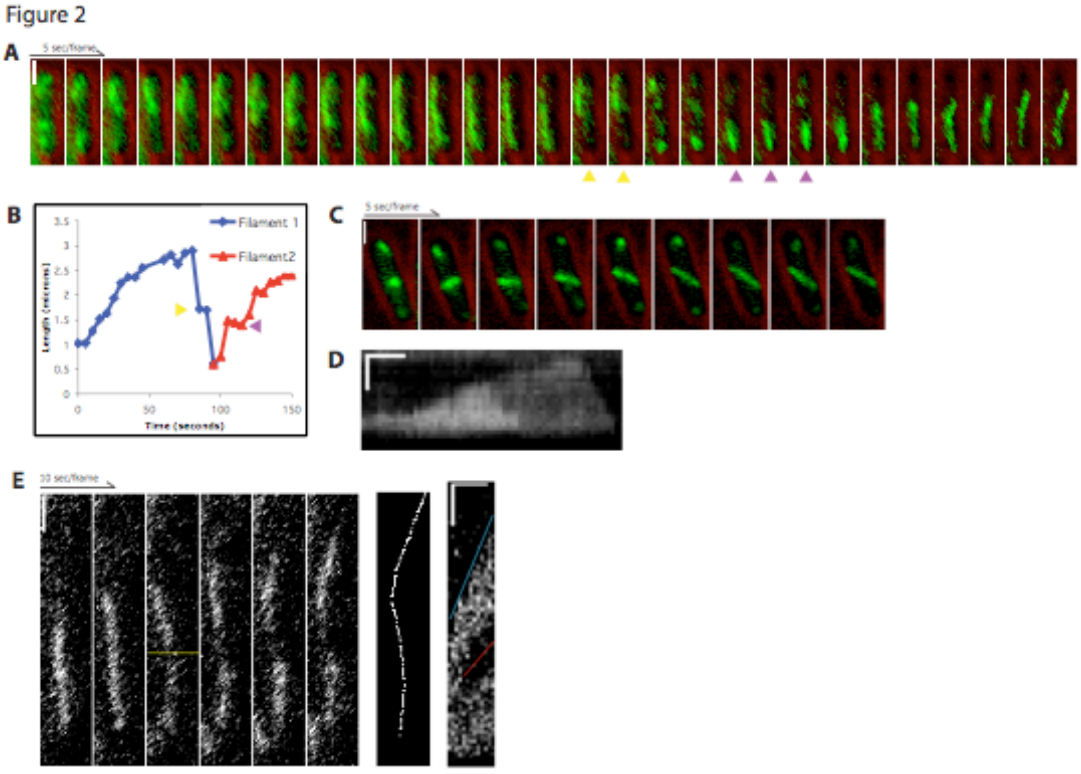


Figure 2.

ParM forms dynamic filaments in E. coli. Time–lapse fluorescence microscopy of live cells expressing GFP-ParM and a plasmid containing the R1 *par* operon. For **A** and **C**, GFP-ParM (green) is superinmposed over single brightfield images (red) taken directly before or after the time series.

(**A**) A ParM spindle polymerizes from one pole to the other, stalls and depolymerizes. A second spindle forms at the opposite pole and polymerizes in the other direction. Due to photobleaching, each frame in the series was contrast adjusted individually.

(**B**) Length of the spindles in **A** measured over time. Pauses can be seen during the depolymerization of the first spindle (yellow arrows) and polymerization of the second spindle (purple arrows).

(**C**) Reorientation of a spindle upon contact with the sides of the cell.

(**D**) Kymograph of a spindle that depolymerizes in two stages. The horizontal bar denotes 20 seconds of elapsed time.

(**E**) Spindles elongate equally from each end. A polymerizing spindle was photobleached to create a fiducial mark (third frame, yellow line). The seventh frame is the line that was drawn to create the kymograph below it. The red line is the rate of displacement of the photobleached spot by polymerization of the left side of the spindle against the end of the bacterium (21 nm/sec). The blue line is the rate of elongation of the entire spindle (44 nm/sec). The horizontal bar in the kymograph denotes 50 seconds of elapsed time. Vertical scale bars are 1$\mu$m. All images were contrast adjusted for clarity and rotated for ease of presentation.

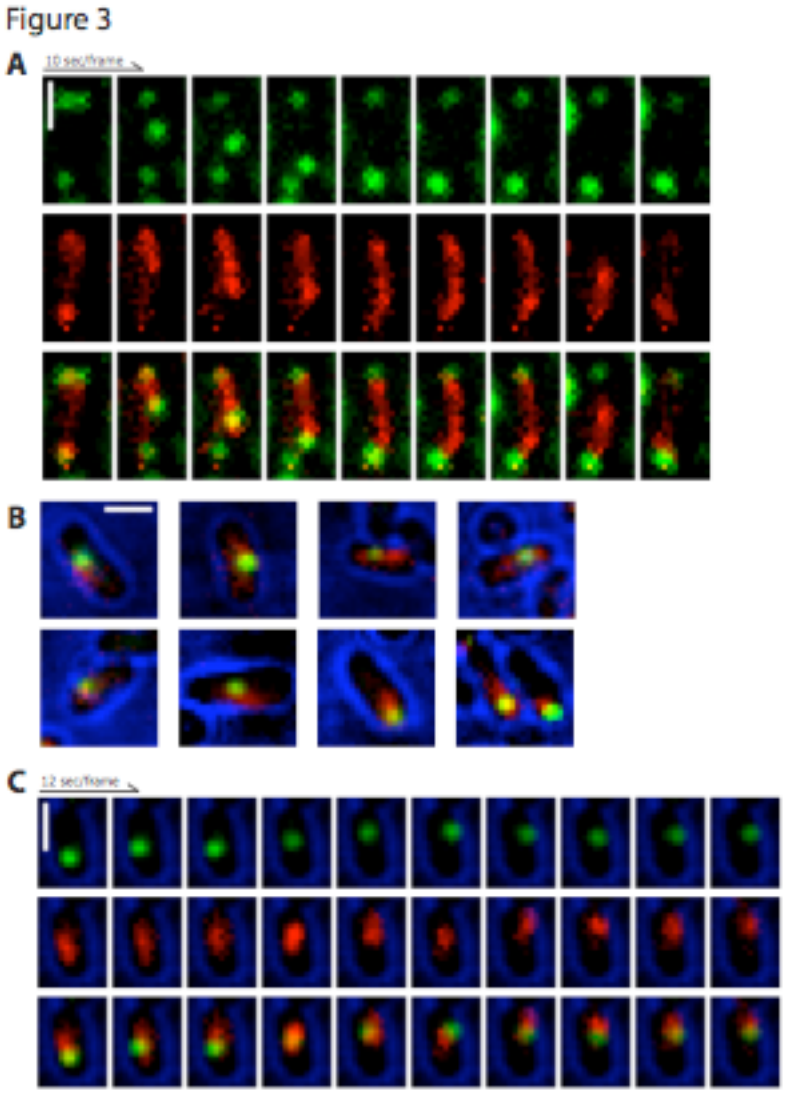


Figure 3.

Near-simultaneous visualization of ParM (red) and plasmids (green).

(**A**) Plasmids co-localize with the ends of spindles as they polymerize across the cell.

(**B**) Co-localization of ParM and plasmids in cells with only one plasmid focus.

(**C**) Time-lapse series of a cell with a single plasmid focus. Brightfield (blue) is a single image taken directly after the time series and superimposed over the fluorescence images.

All scale bars are 1$\mu$m. All images were contrast adjusted for clarity and rotated for ease of presentation.

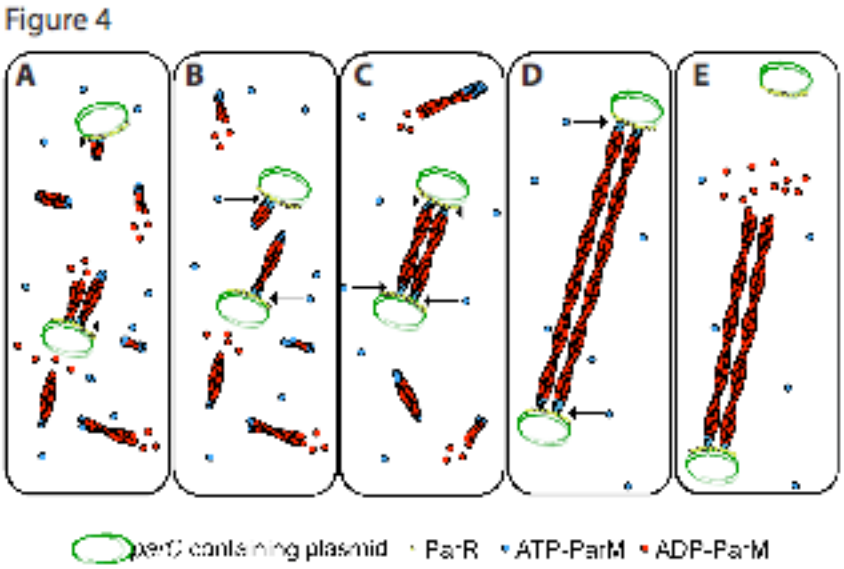


Figure 4. Molecular model of plasmid segregation by the R1 *par* operon.

(**A**) Nucleation of new filaments will happen throughout the cell. Filaments attached to one plasmid will "search" for a second plasmid.

(**B**) Plasmids will diffuse around the cell until they get close enough to encounter each other.

(**C**) When two plasmids come within close proximity, filaments will be bound at each end by a plasmid, forming a spindle. This will prevent the filaments from undergoing catastrophe.

(**D**) As these stabilized filaments polymerize, the two plasmids will be forced to opposite poles. If the ends of a spindle run into the sides of the cell, it will be follow along the membrane to the ends of the cell.

(**E**) After reaching a pole, pushing against both ends of the cell causes the filament to dissociate from the plasmid at one end and quickly depolymerize.

Table 1

| | ParM in vitro | ParM in vivo | Plasmid Segregation |
|---|---|---|---|
| Polymerization rate (nm/sec) | 58 +- 6 | 46 +/- 17 | 52 +/- 17 |
| Depolymerization rate (nm/sec) | 157 +/- 49 | 248 +/- 73 | NA |

Table 1.

Comparison of ParM filament polymerization rates and plasmid segregation rates. Averages +/- Standard Deviations. ParM rates *in vitro* are from Garner and Campbell et. al. 2004. ParM rates *in vivo* were measured from data such as shown in Figure 2. Plasmid segregation rate were measured from clear segregation events such as those seen in Figure 1E and F. ParM polymerization n=22. ParM depolymerization n=9. Plasmid segregation n=22.

# Chapter 5

**Conclusions**

The main conclusions of my graduate work are the following: (1) ParM is dynamically unstable in vitro and in vivo; (2) ParM polymerizes symmetrically from each end; (3) The ParR/parC complex binds to each end of a ParM filament; (4) Plasmid segregation behavior differs with the number of plasmids in a cell; (5) Plasmid segregation by the R1 par operon is a dynamic process that occurs throughout the cell cycle; (6) Plasmid diffusion is slow and corralled absence of the par operon.

The discovery of dynamic instability in ParM was key to our understanding of how the system works. Dynamic instability provides a number of advantages for the system. First, it is a great way to provide turn-over of filaments in the cell. Without constant turn-over of filaments, they would be locked in one state and unable to polymerize when and where they are needed for segregation. By having the two separate states of ADP versus ATP bound actin, it provides an energy difference that allows for constant polymerization. This is seen in the difference between the steady-state concentrations with hydrolysable versus non-hydrolyzable ParM. ParM mutants that cannot hydrolyze ATP have a steady-state concentration of 0.6 micromolar. This is the critical concentration for ParM. If ParM is above this concentration, it will form filaments. Below this concentration, it will not. Since this is the steady-state concentration without ATP hydrolysis, ParM will form polymer but then stall as it comes to equilibrium and cease to form any more filaments. By contrast, when ATP hydrolysis is allowed to occur, the steady state concentration is higher: 2.3 micromolar. The higher

concentration is due to the fact that some of the polymer is now ADP-bound, which has a much higher critical concentration of about 100 micromolar. Since the 2.3 micromolar steady state concentration with hydrolysis is higher than the critical concentration, there will be constant polymerization offset by the occasional rapid depolymerization of unstable, ADP bound filaments. This difference between the steady-state and critical concentration can then be used by Plasmid bound ParM for segregation.

The second advantage is that dynamic instability allows for a search and capture mechanism as has been described for microtubules. Having filaments that can be sent out from one plasmid and grow and shrink at the other end is a more efficient way of searching the cytoplasm than diffusion alone, as the filament dynamics are faster than plasmid diffusion. Additionally, the rapid formation of new filaments throughout the cell could aid in increasing capture rates.

Symetrical polymerization of ParM at each end indicates that there are no differences in the kinetics and thermodynamics of monomer addition to the filaments. For actin, there is a clear preference for monomer addition at the barbed end. The biophysical mechanism for this difference is unclear. The same bonds are being made at both end of the filament, so the differences in Kd are somewhat perplexing. For ParM, this is not an issue, as the Kds for each end of the filament are the same. Potential benefits of this symmetry in ParM are that the plasmids get pushed equally from each end and that the rates of catastrophe are presumably the same. If the polymerization rate at each end of the filament were different, it is likely that the frequency of cap loss would vary accordingly. If this were true, then the searching capabilities of the filaments would be different depending on which end was captured first. This variability would be

potentially disadvantageous, since this parameter is likely fine tuned to maximize capture efficiency.

The fact that plasmids bind to each end of a single filament greatly simplifies the system. Without this mechanism, there would need to be an additional way to make the system symmetrical. For example, in Eukaryotes, the symmetry is made by have two centrosomes on each side of the cell. In ParM, one method might have been to have two antiparralel filaments between each ParR pair. This would require some mechanism to synchronize the two and make things more complicated. Another advantage of binding to each end of a single filament is capture detection. By requiring each end be captured in order to stabilize the filament, there is an inherent mechanism for stabilizing only those filaments that are ready to do useful work in pushing the filaments apart.

One of the most striking observations of par containing plasmids is that the behavior of the plasmids differs greatly depending on whether there are one, two, three, or four plasmids present. One plasmid simply diffuses around the cell. Two plasmids undergo frequent rounds of segregation from each other, with diffusion back together in between. Three plasmids undergo characteristic "ping-pong" behavior where one plasmid goes from pole to pole repeatedly while the other two remain at the poles. With four plasmids, there are many interactions going on and things get complicated. If you measure efficiency of segregation as the percentage of time with at least one plasmid on each side of the division plane, then having three plasmids is much more efficient than having two. In fact, when only two plasmids are present, the system is shockingly inefficient. This may be related to the fact that segregation is only needed at the end of

the cell cycle. By this time, the plasmids have had plenty of time to replicate and will almost certainly have more than two copies per cell.

Another surprising plasmid behavior is the constant segregation throughout the cell cycle. All other know mechanisms of DNA segregation occur right before cytokinesis, which makes sense as that's the only time segregation is actually required to ensure propagation to each daughter cell. So why doesn't the par operon also work in this way? My best guess relies in the simplicity in the system. One theme that kept on occurring in our work on ParM was that it was tuned to function in the absence of regulatory proteins. In a way, this is a continuation of that theme wherein the par operon was tuned to function in the absence of cues from the cell cycle. By constantly segregating the plasmids, it does not further complicate itself by requiring additional inputs from other cellular factors. This is also beneficial for the par operon being able to function properly in a variety of different bacteria. If it does not rely on cellular cues, then it does not have to worry about variations in those cues from cell to cell.

It is not uncommon in science for a simple control to turn into a novel finding. In fact, it seems to be a common occurrence in the Mullins lab. In this case, I aquired a plasmid without the par operon that I could visualize with GFP to compare to the one I had with the par operon. I expected to briefly show that the control plasmid would not have the rapid segregation behaviors. Once I had the movies taken, I realized that they could be further analyzed to get the first detailed measurements of plasmid diffusion in bacteria. As described in the JCB paper, the diffusion was slow and corralled. The slow part wasn't very surprising. Plasmids are huge. On the other hand, the corralling is an indication of something potentially interesting. It is still common for biologists to view

bacteria as little bags of chemicals. Diffusional barriers indicate something far more complex.

**Future Directions**

The one significant hole left in our understanding of how the par operon works is the problem of how the filaments are captured by two different plasmids. Ever since we first came up with our model for a mechanism of segregation, this problem has bothered me. The problem is this: if plasmids are bound and stabilized at one end by each plasmid, where will the other "searching" end bind. These binding sites will already be bound to other filaments. There needs to be an additional mechanism to preferentially bind to filaments that are already bound at the other end. One possibility is that the filaments anneal to each other. End on annealing would be the simplest method, as two filaments that are searching would then become one single filament bound at each end. This mechanism is somewhat difficult to envision as happening on a regular basis. ParM filaments are only about 7 nanometers wide. To find another filament that is equally small, and do it specifically amongst a sea of unbound filaments is highly improbable. Potentially, this process could be aided by side binding between filaments that would guide filaments either to the opposite plasmid or to each other's ends for annealing. Significant side binding has not been seen in vitro and EM images indicate that it is not necessary for capture. Honestly, I have yet to come up with a solution to this problem that seems at all likely to me.

Two questions that I attempted to solve with EM remain allusive: (1) What is the structure of the whole complex together? (2) What is the mechanism of catastrophic

depolymerization? The first question has been made all the more intriguing recently with two structures for ParR indicating that it forms a ring that may fit a ParM filament in the center. A few good images of ParM, ParR and parC together should be able to resolve this issue. As I have outlined my failures with other EM techniques in Chapter 3, I would advise using Cryo EM to best resolve this issue. Question number 2 may also be answered best with Cryo EM. This question has also been made even more intriguing by the ParR structure. The fact that microtubules depolymerize by losing the connection between protofilaments that then curl away has been used as one potential mechanism for how chromosomes remain associated with microtubules during depolymerization. In that case, the Dam1 complex, also shown to form a ring in vitro, is pulled along by the protofilaments. Since plasmids do not remain associated with depolymerizing ParM filaments, it may be that ParM uses a different mechanism for catastrophic depolymerization.

The most appealing area for future directions lies in the many other plasmid segregation systems. All of these other systems contain polymers, such as ParA, AlfA, and TubZ, for which little to no biochemical work has been done. Specifically, the polymer dynamics and polymerization kinetics of these proteins are completely unknown. If there is any greater insight to learn from our work on ParM, it is that such biochemical properties are extraordinarily useful in determining how these systems work.

**Publishing Agreement**

*It is the policy of the University to encourage the distribution of all theses and dissertations. Copies of all UCSF theses and dissertations will be routed to the library via the Graduate Division. The library will make all theses and dissertations accessible to the public and will preserve these to the best of their abilities, in perpetuity.*

***Please sign the following statement:***

*I hereby grant permission to the Graduate Division of the University of California, San Francisco to release copies of my thesis or dissertation to the Campus Library to provide access and preservation, in whole or in part, in perpetuity.*

Chris Cyrus 2/21/08 _____

Author Signature Date